crystals

MDPI

Article

Y-Branched Titanium Dioxide Nanotubes as a Potential Antimicrobial Coating for Implants

Angela Gabriela Păun, Valeria Petrina, Nicoleta Badea, Camelia Ungureanu, Simona Popescu and Cristina Dumitriu *

Faculty of Chemical Engineering and Biotechnologies, The National University of Science and Technology Politehnica Bucharest, Gh. Polizu 1–7, 011061 Bucharest, Romania; angela.olaru@upb.ro (A.G.P.); valeria_14694@yahoo.com (V.P.); nicoleta.badea@upb.ro (N.B.); camelia.ungureanu@upb.ro (C.U.); simona.popescu@upb.ro (S.P.)
* Correspondence: cristina.dumitriu@upb.ro

Abstract: The early loss of dental implants can be avoided with systemic antibiotics, however there are potentially significant side effects. Consequently, the use of local drug administration techniques is necessary to make dental implant therapy more practical. In this study, Y-branched nanotubes were prepared by non-expensive and simple anodization in two steps. Tests were performed to highlight their potential for local antibiotic administration. Y-branched nanotubes were able to incorporate a dose of Tetracycline and ensure its electrochemical stability. The presence of tetracycline significantly enhanced antibacterial efficacy, resulting in an increase of up to 55% for *Escherichia coli* and *Pseudomonas aeruginosa* and 50% for *Staphylococcus aureus*. The comparable antibacterial effects of the nanostructured surfaces highlight the potential of tetracycline in promoting antimicrobial action. Moreover, the addition of tetracycline does not influence the structural, morphological and stability properties of the nanostructured deposited TiO_2 films.

Keywords: Y-branched nanotubes; tetracycline; antibiotic release; antibacterial effect

Citation: Păun, A.G.; Petrina, V.; Badea, N.; Ungureanu, C.; Popescu, S.; Dumitriu, C. Y-Branched Titanium Dioxide Nanotubes as a Potential Antimicrobial Coating for Implants. *Crystals* **2023**, *13*, 1695. https://doi.org/10.3390/cryst13121695

Academic Editors: Shrikant Joshi, Thomas Lampke and Thomas Lindner

Received: 22 November 2023
Revised: 14 December 2023
Accepted: 15 December 2023
Published: 17 December 2023

1. Introduction

One of the implant failures, peri-implantitis, could be developed because of an immune response to oral cavity microbes. Once peri-implantitis has manifested, the focus should be on cleaning the implant surfaces, addressing swelling, and preventing additional bone loss [1].

Titanium and its alloys are commonly employed materials in the medical field due to their advantageous properties, including biocompatibility, corrosion resistance, and mechanical strength. However, titanium lacks intrinsic antibacterial properties, leading to limited osseointegration. Therefore, surface modification becomes essential to stimulate osteogenesis and establish favorable interfacial microenvironments at the implant-bone tissue interface [2–4].

Nanotechnology has made significant improvements in the creation of antimicrobial coatings that could be employed to prevent implant infection [1]. Various novel nanomaterials and drug carriers, including polymer micelles, liposomes, multifunctional dendritic polymers, nanocapsules, nanospheres, and TiO_2 nanostructures have been created as a result of advancements in nanotechnology [5,6].

TiO_2 nanotubes (NT) have drawn a lot of attention in recent years as a potential material to enhance osseointegration and as a potential medication delivery method [7]. The clinical therapeutic effect of medical implants can be enhanced by titanium nanotubes arrays produced on Ti surface by an easy electrochemical anodizing technique [5]. Biocompatibility investigations of TiO_2 nanotubes have predominantly centered on their application in dentistry, orthopedics, and cardiovascular surgery. Notably, NT implants have exhibited a strong affinity for bone cell adhesion and differentiation. Initial studies revealed that

NT surfaces promote bone cell growth and enhance osteoblast activity. Many researchers demonstrated the favorable effects of NT surfaces on the growth and differentiation of bone marrow stromal cells, presenting the potential for controlling nanotopography to enhance osteoblast activity. Other studies highlighted increased proliferation of osteosarcoma and MC3T3-E1 cells on NT surfaces. It was also used as a protozoan cell model to predict NT coating toxicity in biological systems, concluding that NTs did not adversely affect esterase activity or cell growth rate. In vivo studies, involving NT implants in pigs, demonstrated improved osteoblast functions and resistance to shear forces during implant insertion, highlighting positive bone formation characteristics. Other researchers reported increased chondrocyte adhesion on NT surfaces, with in vivo biocompatibility studies in rats showing no chronic inflammation or fibrosis upon subcutaneous implantation. Moreover, in vivo studies on rabbit tibiae, confirmed that NT implants significantly enhanced the strength of the bone bond with surrounding tissues [8–12].

Furthermore, double-layer nanotube arrays were created, featuring branching nanotubes growing beneath the trunk nanotubes through the anodization process [13]. Benefits of these structures include an enhanced specific surface area and biocompatibility [14,15]. Also, mouse bone marrow stromal cells adhered to, multiplied, and differentiated on the surfaces of double-layered titania nanotubes [15]. Titanium nanotubes have not been observed to generate inflammation or fibrous vesicles in vivo, demonstrating that they do not elicit a potent immunological response [16]. Notably, the reagent itself and its local concentration determinate the toxicity brought by the loading of the reagent. Controlling the release of reagent become essential [16]. However, there does not seem to be agreement yet on the ideal nanotube morphology to encourage cellular adhesion and proliferation as well as efficient drug delivery [17]. NT surfaces offer the benefit of loading drugs or active agents for localized delivery. These tubular structures play a direct role in interactions with cells, and their biocompatibility and capacity to differentiate into specific cell types can be enhanced through the incorporation of specific growth factors [3]. Hence, the advancement of antimicrobial implants is vital to ward off dental infections and mitigate the risk of early treatment failure. In the effort to combat infections, NT surfaces can be loaded with an array of antibacterial agents such as antibiotics, metal oxides or ions, and antimicrobial peptides, facilitating localized action [18].

Tetracycline, a protein synthesis inhibitor, attaches to the bacterial ribosome subunit and prevents the interaction of tRNA and mRNA. Notably, tetracycline has shown that, in addition to being a potent broad-spectrum antibiotic against bacteria linked to periodontitis and periimplantitis, it also increases the proliferation of fibroblastic cells and inhibits collagenase activity [19]. Thus, bacteria, such as *Prevotella intermedia/nigrescens*, *Fusobacterium* sp. *Bacteroides forsythus*, and *Campylobacter rectus* are less frequently developed when this chemical is present [19]. Because of its beneficial effects on bone graft materials, ability to regenerate bone in extraction sockets, and other mentioned properties, tetracycline is frequently employed in the regeneration process [20]. Moreover, considering cell interactions, literature studies indicate that loading tetracycline into TiO_2 nanotubes does not have adverse effects on cell adhesion, proliferation, and differentiation [15,21].

Systemic antibiotics are effective in preventing the early loss of dental implants, but studies point out serious shortcomings related to restricted drug solubility, short circulating time, lack of selectivity, side effects varying from diarrhea to potentially fatal allergic responses, and unfavorable pharmacodynamics [5,15]. Additionally, there is a general agreement that systemic antibiotics are overused in dental care. Research into local drug administration methods has shown demonstrable efficacy in reducing infection rates [7,22]. The interaction between antimicrobial coatings and bacteria is a topic of extensive research, especially for developing antibacterial surfaces and materials to reduce the risk of infections [1].

This research aimed to investigate Y-branched titanium nanotubes for use in commercial orthopedic implants with strong antibacterial qualities. Immersion drug loading was used in this study to incorporate Tetracycline into Y-branched TiO_2 nanotubes, which

were then examined using in vitro techniques on two Gram negative bacteria, (*Escherichia coli* and *Pseudomonas aeruginosa*) and one Gram positive, (*Staphylococcus aureus*). Further research was completed to see whether the treated tube layers had better antibacterial effectiveness and longer drug release.

2. Materials and Methods

2.1. Reagents

Ethylene glycol—anhydrous (EG—99.8% purity), ammonium fluoride (NH_4F), sulfuric acid (H_2SO_4), dimethylsulfoxide (DMSO) and natrium chloride (NaCl) were provided by Sigma Aldrich.

2.2. Fabrication of Two Layered TiO_2 Nanotube Arrays

Two-layered anodic titanium dioxide (TiO_2) nanotubes with a 'Y' branched structure were produced through a two-step anodization process of Ti samples. Before anodization, the Ti samples with a thickness of 1 mm and a 99.6% purity, provided by Good Fellow Ldt., were polished using abrasive papers of different granulometry (Carbimet, Buehler) and then were cleaned in distilled water and degreased in ethanol, and acetone, respectively [18,23,24], at room temperature.

The anodization process was performed in an electrochemical cell with two-electrode, with Ti electrode as anode and a Pt electrode as cathode. Using a MATRIX MPS-7163 source, the voltage was increased from 0 to the final value specified in Table 1, with 2 V/10 s and then kept constant at room temperature for 2 h. A digital multimeter (from V&A International, model VA18B, with PC-Link version 7 software) connected to the computer was used to record the evolution of the current during anodization.

Table 1. The parameters used for obtaining the "Y" branched TiO_2 nanotubes.

Sample	Steps	Electrolyte Composition	Voltage (V)	Time (h)	Sample Name
Anodization to obtain simple nanotubes	1	NH_4F (0.5% wt) + distilled water (2% v) + EG	50	2	NT_1s
Anodization to obtain "Y" branched nanotubes	1	Aqueous solution: H_2SO_4 1 M + 0.16 M HF	20	2	NT_2s
	2	NH_4F (0.5% wt) + distilled water (2% v) + EG	20	2	

The parameters of the anodization process are presented in Table 1. The sample anodization in one step used an organic electrolyte based on ethylene glycol. Conversely, the two-step process involved initial anodization in a non-organic, followed by anodization in an organic electrolyte.

The anodized titanium samples were sonicated with deionized water and then dried in the ambient atmosphere. These were named NT_1s and NT_2s.

2.3. Tetracycline Loading

For antibiotic embedding into TiO_2 nanotubes, firstly, a tetracycline solution of with a 2 g/L concentration was prepared. Due to the low stability of this antibiotic in water, a solubilization protocol was employed using a mixture of ethanol and distilled water in a 3:1 ratio.

The anodized samples (NT_1s and NT_2s) were immersed in 10 mL of tetracycline solution for 48 h at room temperature. Tetracycline loaded samples were named NT_1s/TE, NT_2s/TE.

The entrapment efficiency of tetracycline (EE) was calculated using the equation:

$$\%EE = \frac{W_a - W_s}{W_a} \times 100 \quad (1)$$

where Wa = weight of total drug used for immersion solution (20 mg); Ws = analyzed weight of solution after loading.

The quantity of tetracycline unencapsulated was determined using a calibration curve with a correlation coefficient (R2) of 0.9998 and a linear regression equation of $y = 0.0345 \times -0.0013$ with a concentration between 4–20 mg/L tetracycline. All the tests were executed in triplicate ($n = 3$).

2.4. Samples Characterization

The samples were morphological, structural and electrochemical characterized. Surface morphology was analyzed using scanning electron microscopy (SEM). Top and cross-sectional views were obtained with a FEI/Philips XL-30 QUANTA 650 in high vacuum, at HV 30 kV, WD 10 mm (FEI Company, Hillsboro, OR, USA), at different magnifications. Cross-sectional images were performed by mechanically scratching the anodized electrodes with a scalpel to crack the nanotube layer.

Information about crystallinity and functional groups was obtained using Raman technique. The Raman spectra for nanotube samples was obtained at a wavelength of 514 nm and 785 nm for samples loaded with tetracycline.

Surface wettability was investigated using a CAM 100 Optical Contact Angle Meter (KSV Instruments Ltd., Helsinki, Finland), employing the Sessile Drop method in three different solvents (water, EG and DMSO). The contact angle value was measured three times in different areas on the sample surface at room temperature and under daylight conditions. The surface energy was calculated using the model of Owens DK and Wendt R, as described in the literature [25].

The electrochemical characterization of the samples was performed in a cell with three electrodes (working electrode—simple Ti or coated Ti electrode; reference electrode—Ag/AgCl/3M KCl; counter electrode—Pt). Electrochemical measurements were carried out with a potentiostat/galvanostat device model PGSTAT 302N (Autolab), using Nova 1.10 software.

Tafel polarization curves were recorded in the range ± 150 mV compared to the open circuit potential, in 0.9% NaCl solution, under ambient conditions. The scanning rate was 2 mV/s. From Tafel plots, corrosion parameters were determined using Nova 1.11 software and protection efficiency was calculated using the following equation:

$$\text{Protectionefficency} = \frac{\left(I^0_{corr} - I_{corr}\right)}{I^0_{corr}} \cdot 100 \quad (2)$$

where I^0_{corr} is the corrosion current of the Ti substrate and I_{corr} corrosion current of the modified samples.

Moreover, electrochemical impedance spectra (EIS) were recorded, with an amplitude of 10 mV, in the range 0.1–10^5 Hz, at free potential value and room temperature. The data were processed using Nova 1.11 to determine the equivalent electrical circuits and generate Nyquist diagrams. Cyclic voltammetry curves were recorded in the range (−1.5 V; 1 V), with a step of 2.44 mV and a scanning rate of 100 mV/s.

2.5. Tetracycline Release Evaluation

For release studies, NT_1s and NT_2s samples were immersed in tetracycline solution at a concentration of 2 g/L for 48 h.

Following that, the samples were immersed in a 10 mL phosphate buffer (pH = 7.4). Each time, 0.5 mL of solution was extracted from the medium and replaced with an equal volume of PBS. The concentration of drug released over time in the buffer solution was assessed via UV–VIS spectroscopy at a wavelength (λ) of 363 nm, according to the method described in point 2.3.

To study the release kinetics and determine the mechanism of drug release, the results of the in vitro tetracycline release study were adjusted using several kinetic models. All the tests were executed in triplicate (n = 3).

2.6. Bacterial Culture

Bacteria were grown at 37 °C [26] on autoclaved Luria Bertani Agar (LBA) acc. Miller plates. A quantitative method was used to assess the tested samples' antibacterial activity against test bacteria, and the result was the percentage inhibition of growth (or Bactericidal ratio), or PI%. [27]:

$$PI\ \% = [(M_{18} - M_0) - (S_{18} - S_0)]/(M_{18} - M_0) \times 100, \quad (3)$$

where PI represent the growth inhibition percentage, M_{18} is the optical density at 600 nm (OD_{600}) that has been blank-compensated, M_0 is the blank-compensated OD_{600} of the organism's positive control at 0 h, S_{18} is the OD_{600} of the organism that has been negatively corrected for the presence of a test sample at 18 h, and S_0 is the negatively corrected OD_{600} of the organism at 0 h.

In summary, sterile samples were incubated in a Laboshake Gerhardt shaker at 37 °C and 200 rpm for 18 h using 5 mL of Luria–Bertani broth (the sterile medium was inoculated with bacteria at an amount of 1%). Using a UV–VIS spectrophotometer (Jenway Spectrophotometer), the optical density of the samples and the control (a bacterium culture without sample) was measured at 600 nm to evaluate the bacterial growth.

Antibacterial assay was performed against three pathogenic bacteria: two Gram negative, (*Escherichia coli* and *Pseudomonas aeruginosa*) and one Gram positive, (*Staphylococcus aureus*) for the reasons mentioned in the Section 1. The method used is a quantitative one and is described in the paper [28]. All reagents were purchased from VWR International (Graumanngasse, Vienna).

Analysis of variance (one-way ANOVA) and the Tukey test were used to examine statistical significance of the results obtained by triplicate determinations (described for each method). Significant differences between means were found. At $p < 0.05$, differences were considered significant. The findings displayed for the calculations are the mean ± standard error of the mean (SE) of separate calculations. All of the graphic representation was created using OriginPro 2010 Data Analysis and Graphing Software v. 8.5 (OriginLab Corporation, Northampton, MA, USA).

Nosocomial infections are an important aspect of the infectious potential of the bacterium and may include any of the pathologies already listed but have the characteristic spread in hospitals and health institutions, with frequent involvement of multidrug-resistant strains.

3. Results and Discussion

3.1. Anodization curve

Titanium surface modification with nano-architectural structures, specifically in the form of nanotubes, is highlighted by observing changes in current intensity over time. Figure 1 shows these curves corresponding to each type of sample, NT_1s and NT_2s.

In literature studies [29], it has been demonstrated that by gradually increasing applied voltage from the beginning of anodization process, the destabilization of the equilibrium state inside the pores is avoided, by galvanostatic method. Thus, all anodized samples were made using a current source, with a gradual increase in applied voltage of 2 V/10 s.

Figure 1 shows the mechanism by which nanostructures are formed under different conditions. The chronoamperometric curve, corresponding to the nanotube's growth in both one-step and two-step methods, comprises distinct stages. The behavior is typical for electrolytes with F^- ions, like that described in the literature [30]. The kinetic trend is composed of three stages, regarding to the current variation: an initial rapid decline (stage A), a gradual increase (stage B), and a quasisteady state current density (stage C). During stage A, the anodizing process initiates, causing a rapid decrease in current to a

minimum value. This reduction is a result of the formation of a high-resistance compact oxide layer on the surface, which occurs through the interaction between Ti^{4+} ions and oxygen O^{2-} ions in the electrolyte. During stage B, the current presents a steady increase to a maximum level as the process of pore formation advances. This is attributed to the chemical dissolution of the oxide layer facilitated by fluoride ions, which is favored by an electric field generated between the cell electrodes. Small pits emerge on the compact layer surface, leading to the development of a nanoporous structure. In the final stage, the current density stabilizes at a constant value as a steady state is achieved, indicating the formation of TiO_2 nanotubes [31].

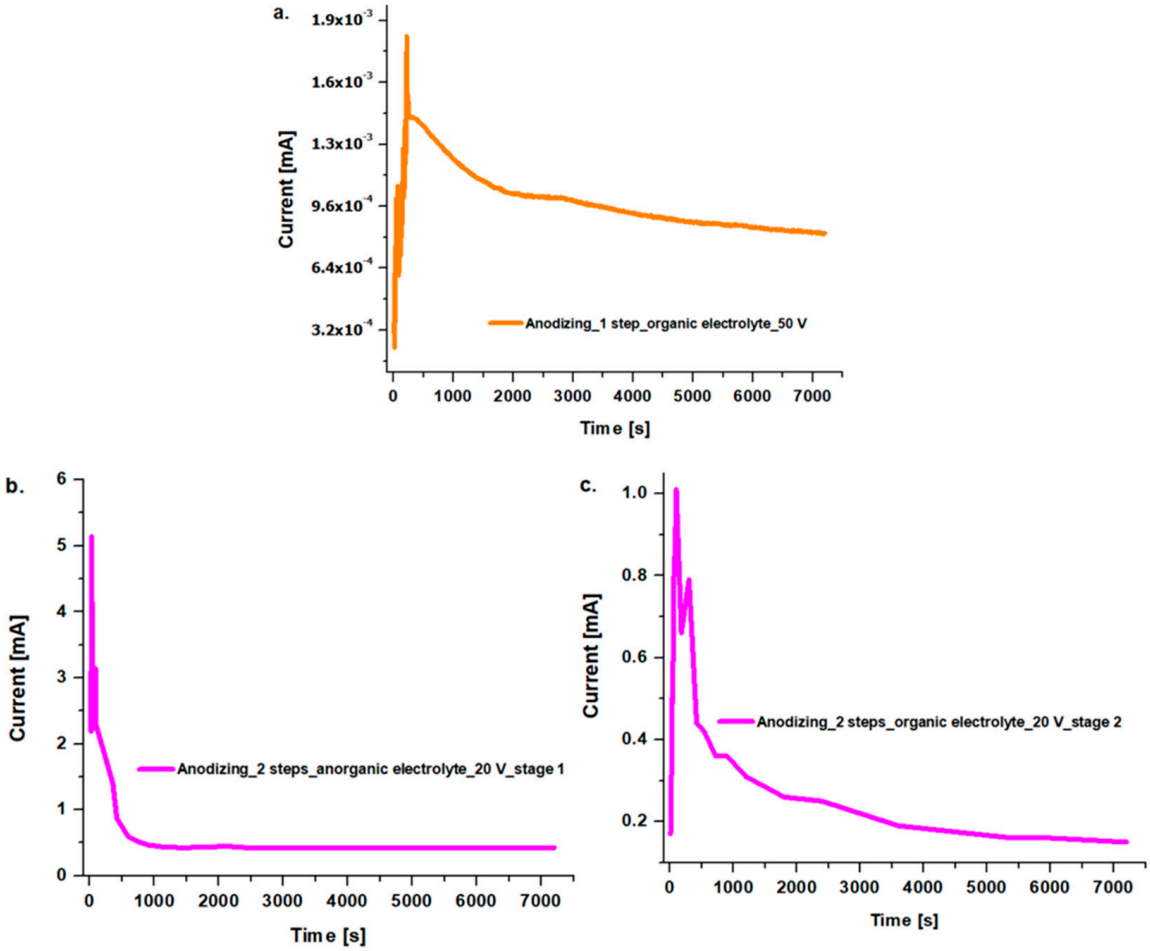

Figure 1. Current—time curves recorded during anodization process: (**a**) NT_1s; (**b**,**c**). NT_2s.

For one-step anodization (Figure 1a), the recorded currents are lower than in two-step sample anodization (Figure 1b,c). For two-step anodization, where an oxide layer is already present on the Ti surface, the currents corresponding to stage 2 (Figure 1c) are notably lower. Also, in Figure 1c, between 180–3600 s, the current increases and decreases, in accordance with the mechanism described in the literature [30]. This behavior corresponds to the second layer, where pits form at the bottom part of the nanotubes obtained in the first layer, followed by their random dissolution.

By integrating the area under the time—current intensity curve for the entire anodization process, using the OriginPro 8.5 software, the load values were obtained. When anodization process was performed to obtain the monolayer nanotubes (NT_1s), the resulting load was about 7 Coulombs (C). For multilayer nanotubes (NT_2s), in the 1st stage the resulting load was 3 C and in the second one, 2 C, resulting in a total of 5 C. Although the titanium surface subjected to anodization was the same, the difference obtained is due to

different parameters of anodization. This difference is in accordance with literature data, describing different mechanisms for the two types of anodization process [13].

3.2. Structure and Morphology of Samples

Figure 2 shows the SEM images of the anodized samples: in one step with and without tetracycline (NT_1s and NT_1s/TE). Before the SEM images were recorded, the samples were scratched to see the nanotubes in the section. In Figure 2b, the cross-section layer of NT_1s is visible. In Figure 2a, can be seen the inner diameter of the nanotubes with a value of about 67 nm and the outer diameter, with values approximately 90 nm. It is also observed that nanotubes are ordered, vertically aligned and uniformly distributed. Viewed from above, these nanotubes have a porous structure, with ordered pores, like "honeycombs".

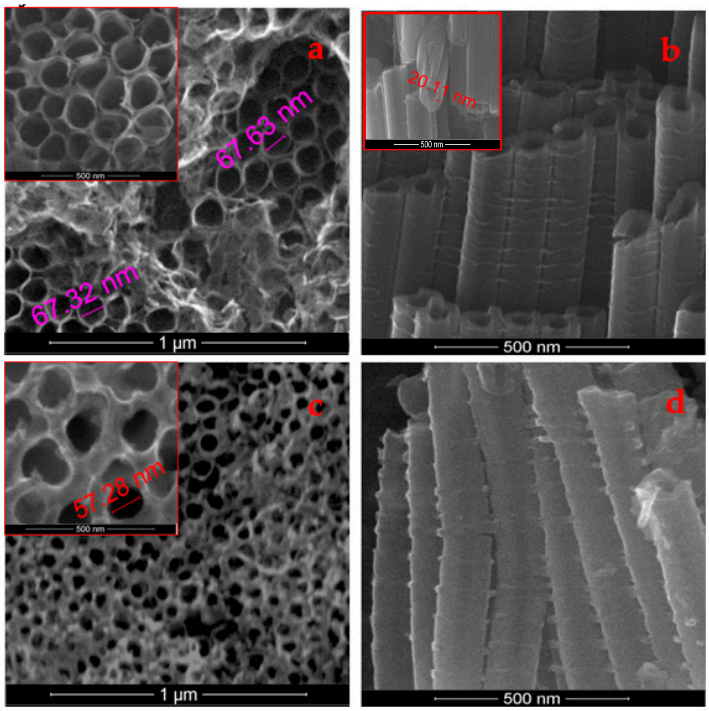

Figure 2. SEM images of anodized samples: (**a**,**b**) NT_1and (**c**,**d**) NT_1s/TE.

Figure 2c,d shows the SEM images of the NT_1s samples in which tetracycline was loaded, resulting NT_1s/TE sample. It is visible that tetracycline does not influence the morphology of nanotubes. Tetracycline incorporation slightly reduces the inner diameter of the nanotubes, 57 nm, (Figure 2c) compared to the SEM images described above in Figure 2a (67 nm), indicating that it was successfully attached to the nanostructured surface.

In Figure 3a–c, the branched morphology of NT_2s can be observed, with values of outer diameters between 98–155 nm and the inner diameter, with values of approx. 60 nm. These morphological changes are also visible in the anodizing curve (according to Figure 1). The difference between the two types of nanotubes (NT_1s and NT_2s) manifests itself also at the level of the nanotubes wall thickness: NT_1s has values of 20 nm (Figure 2b) versus NT_2s, that is 35 nm (Figure 3b), being visibly thicker. From these images, the nanotubes are self-organized and oriented vertically, being open at the top part and closed at the bottom. The length of the nanotubes is closely related to the working conditions. In the literature it has been shown that the length of the obtained nanotubes increases proportionally to the applied voltage [32]. In both cases, the length of the nanotubes is in the order of micrometers.

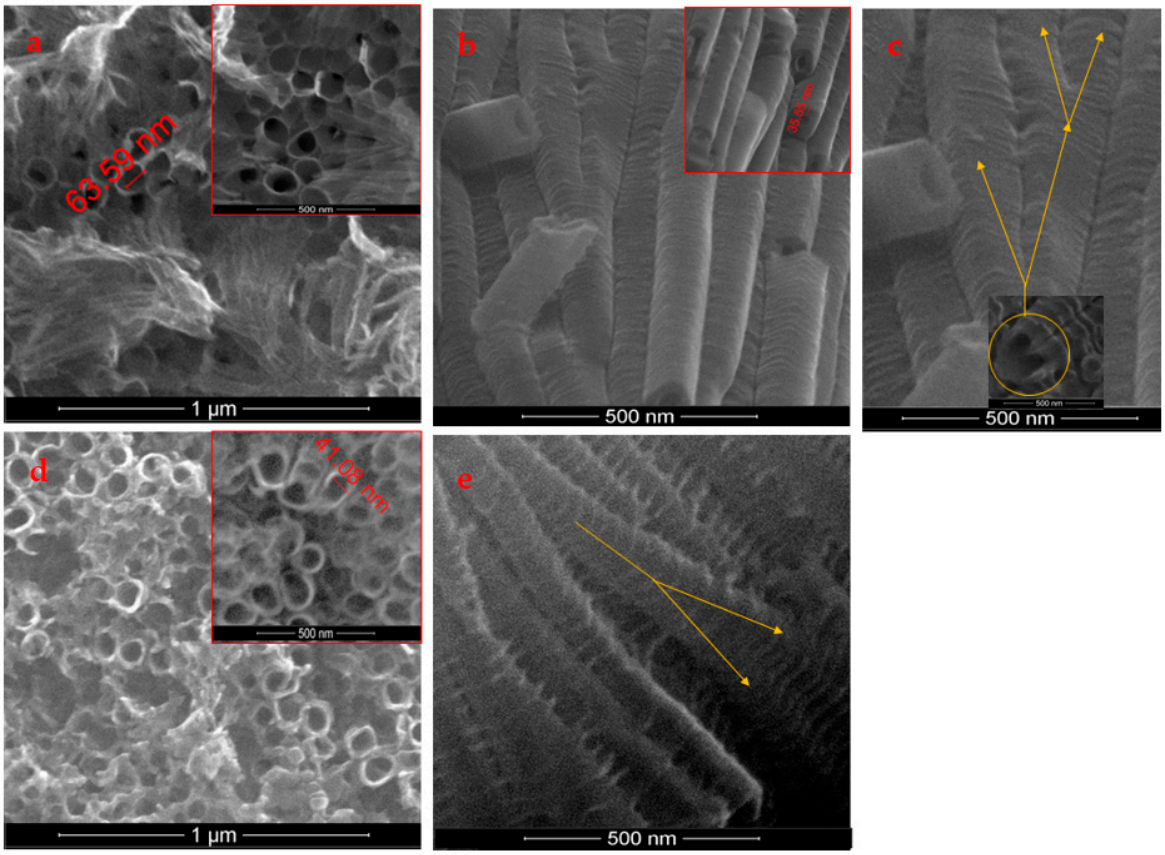

Figure 3. SEM images of tetracycline samples: (**a**–**c**) NT_2s and (**d**,**e**) NT_2s/TE.

Figure 3d,e shows the SEM images of the NT_2s samples in which tetracycline was loaded, resulting in the NT_2s/TE sample. The morphology of nanotubes remains unaffected by the presence of tetracycline, as it can be observed in the images. The inclusion of tetracycline results in a slight reduction in the inner diameter (41 nm) of the nanotubes (Figure 3d) when compared to the SEM images detailed in Figure 3a (63 nm). This suggests successful tetracycline attachment to the nanostructured surface.

For each sample, 20 nanotube diameters were measured using the ImageJ program. Then, the average value and standard deviation for all sample diameters was calculated using Excel. The values obtained for the samples are: NT_1s-67.90 ± 2.21, NT_2s-61.17 ± 2.94, NT_1s/TE-56.61 ± 3.81 and NT_2s/TE-42.75 ± 4.00. Considering these small values for the standard deviations, it is evident that all the samples have uniform TiO_2 nanotube surfaces.

3.3. Raman Characterization

Figure 4 shows the Raman spectra of the samples: (a) TiO_2 A, (b) TiO_2 R, (c) NT_1s, (d) NT_2s, (e) TE, (f) NT_1s/TE, (g) NT_2s/TE. Compared to controls (Figure 4a,b), the anodized samples have both anatase and rutile peaks. The representative peaks of the TiO_2—rutile are found at 108.33 cm^{-1}, 239 cm^{-1}, 440 cm^{-1}, 602 cm^{-1} and at 693 cm^{-1}, and for TiO_2—anatase are around 144 cm^{-1}, 394 cm^{-1}, 514 cm^{-1} and 637 cm^{-1} [33]. Four distinct Raman active modes of anatase TiO_2, characterized by symmetries Eg, B1g, A1g, and Eg, were identified at 141, 392, 511, and 635 cm^{-1}, respectively. The presence of these characteristic vibrational frequencies and their intensity ratios serves as confirmation of the phase-pure anatase TiO_2. Conversely, rutile TiO_2 exhibited stretching peaks at 110, 436, and 590 cm^{-1}, corresponding to the symmetries of B1g, Eg, and A1g, respectively. Additionally, a broad compound vibrational peak at 233 cm^{-1}, arising from multiple phonon scattering processes, was distinctly observed [34].

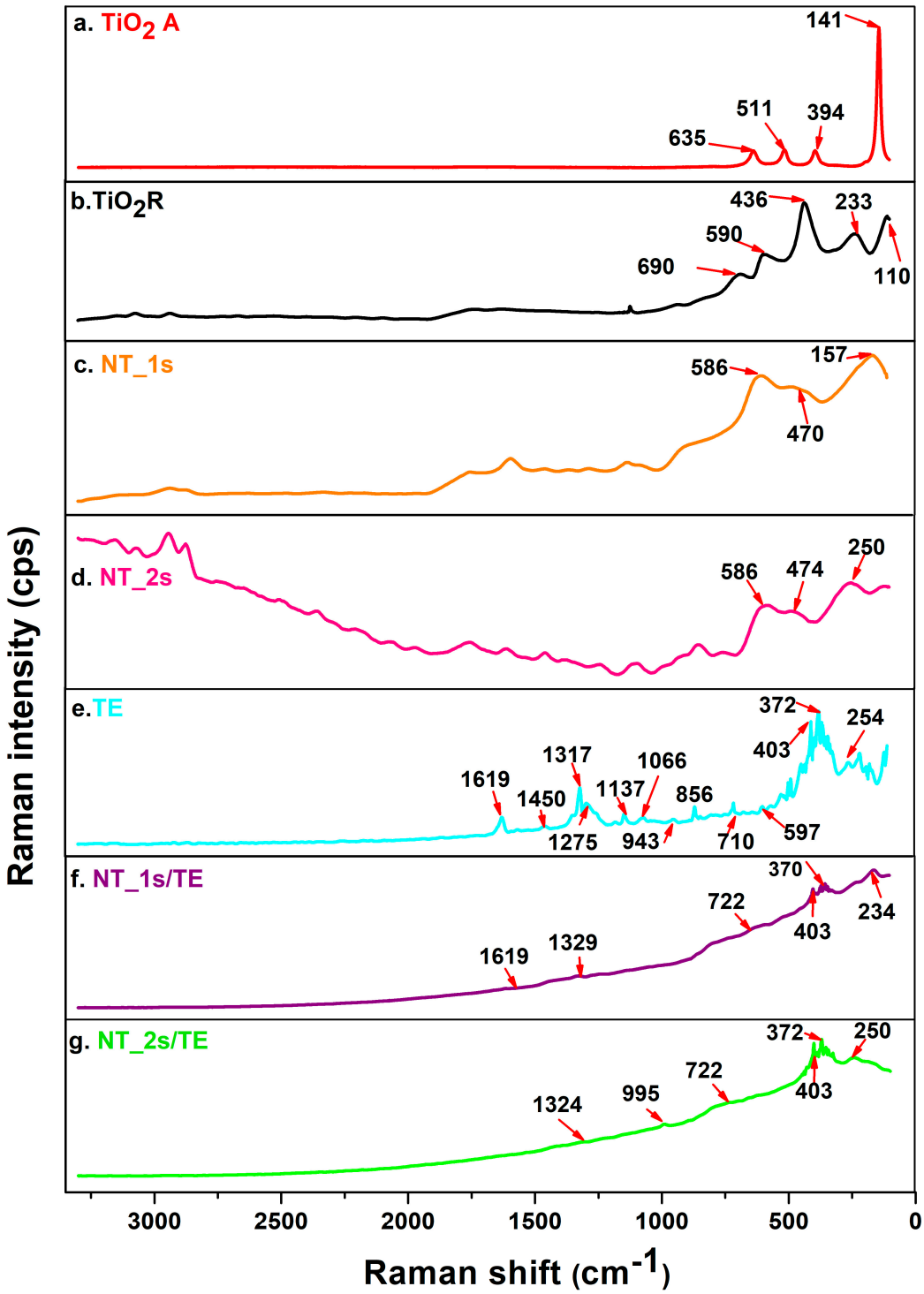

Figure 4. Raman spectra of the samples: (**a**) TiO_2 A, (**b**) TiO_2 R, (**c**) NT_1s, (**d**) NT_2s, (**e**) TE, (**f**) NT_1s/TE, (**g**) NT_2s/TE.

For NT_1s (Figure 4c), the values of the peaks are comparable to those of the rutile (Figure 4b), the same situation being observed for the NT_2s sample (Figure 4d). The peak intensity for NT_2s is lower than for NT_1s.

In Figure 4e, tetracycline shows Raman spectral peaks at 1619, 1450, 1317, 1275, 1137, 943, 856, 710, 597, 497, 403, 372 and 254 cm^{-1} [35,36]. Raman spectra corresponding for anodized samples immersed in the tetracycline solution are presented in Figure 4f,g. These show characteristic peaks for both tetracycline and TiO_2 allotropic forms. It can be observed

that the NT_1s/TE, NT_2s/TE and TE powder present similar peaks, thus indicating that tetracycline was incorporated on the NT_1s and NT_2s surfaces.

3.4. Wettability

Wettability and surface chemistry are important features for tissue-implant interaction. Thus, all samples underwent wettability testing using three different solvents, as seen in Table 2. Ti sample exhibits the lowest hydrophilicity, as indicated by a contact angle value of 84° in water, which is below the threshold of 90°. The anodization process and formation of the nanotubular structure on the Ti surface leads to a decrease in the contact angle. The contact angles values using water as solvent are almost similar since, they present similar top surface morphologies. This correlation is consistent with the observations made in SEM images. Regarding the surface chemistry there are no differences as in the second step the electrolyte solutions are the same for both anodized samples. NT_1s is 29°, and NT_2s is 24.5°. The tetracycline encapsulation in the two samples leads in both cases to the decrease in the contact angle. These have the following values: 17.6° for NT_1s/TE and 23.4° for NT_2s/TE, slightly lower values after embedding the tetracycline.

Table 2. Values for contact angle and surface energy.

Samples	Contact Angle (°)			Surface Energy mJ/m^2
	Water	Ethylene Glycol	DMSO	
Ti	84 ±1.5	43.9 ± 2	33.7 ± 0.1	39.76
NT_1s	29.5 ± 1	22.6 ± 0.5	16.6 ± 2	63.25
NT_2s	24.5 ± 0.08	14.7 ± 1	10.7 ± 0.2	66.25
NT_1s/TE	17.6 ± 0.4	16.6 ± 0.1	14.8 ± 0.2	73.43
NT_2s/TE	23.4 ± 0.1	19.1 ± 0.2	14.3 ± 0.1	67.11

The surface energy increases for the modified samples. Tetracycline samples (NT_1 s/TE and NT_2s/TE) show the highest surface energy.

3.5. Electrochemical Characterization

3.5.1. Tafel Diagrams

To assess the resulting modified Ti biocorrosion resistance, electrochemical tests were conducted on it in the 0.9% NaCl solution. Tafel polarization curves were recorded using Nova software, version 1.11 and are presented in Figure 5. This figure depicts the formation of passive films for all the anodized samples.

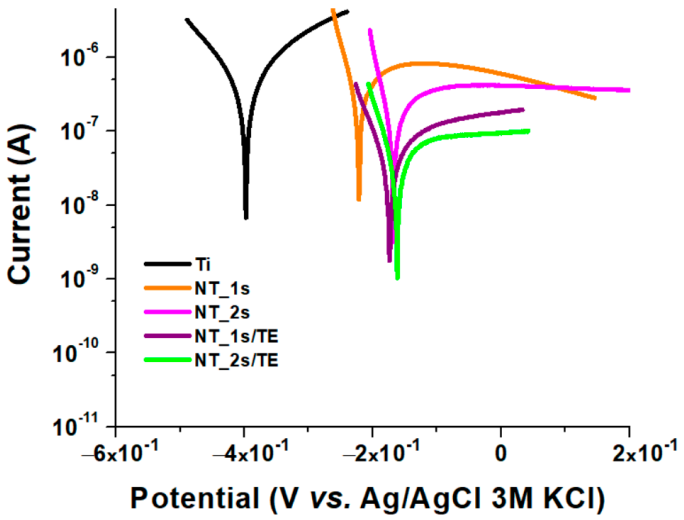

Figure 5. Tafel diagrams of the analyzed samples.

By analyzing these curves with specific software, the corrosion parameters were determined: corrosion potential (E_{cor}), corrosion current (I_{cor}), corrosion current density (i_{cor}), corrosion rate (v_{cor}). The results are presented in Table 3.

Table 3. Values obtained from measurements from the Tafel analyses.

Parameters	Samples				
	Ti	**NT_1s**	**NT_2s**	**NT_1s/TE**	**NT_2s/TE**
E_{corr} (V)	−0.398	−0.221	−0.167	−0.174	−0.161
I_{corr} (A)	6.54×10^{-7}	2.25×10^{-7}	1.48×10^{-7}	1.10×10^{-7}	0.43×10^{-7}
Corrosion rate (mm/year)	7×10^{-3}	3×10^{-3}	2×10^{-3}	10^{-3}	4×10^{-4}
Protection Efficiency (%)	-	66	77	83	93

E_{corr} is an important parameter when corrosion is evaluated. The anodized samples provide enhanced corrosion protection, displaying reduced susceptibility to corrosion compared to Ti samples. This improvement is attributed to the surface modification with nanotubes, causing a shift in the corrosion potential towards higher electropositive values. The obtained values and observed behavior align with the results from our previous studies on titania nanotubes [3]. Additional research revealed that the nanotube layer form a robust ceramic barrier that protect the metallic substrate from corrosive environments [37]. The NT_2s/TE sample is passivizing demonstrates at more electropositive potential values compared to Ti substrate and bare nanotubes. This indicates its enhanced thermodynamic stability. Thus, it can be stated that tetracycline does not disturb the corrosion behavior of nanotubes.

Higher corrosion current (I_{corr}) values imply a weaker corrosion resistance, while lower corrosion resistance is often indicated by lower corrosion current (I_{corr}); I_{corr} values being directly proportional to the corrosion rate. The modified samples show a much lower corrosion current. For the NT_2s/TE sample, it is one order of magnitude lower than Ti.

As seen from Table 3, Ti has the highest value of corrosion rate, 0.007 mm/year. The corrosion rate decreases by about an order of magnitude. This can be explained by the semiconductor nature of titanium oxide. This oxide acts as a protective layer on titanium, creating a thick shield that stops the diffusion of titanium ions and oxygen ions.

The protection efficiency is high—above 60%, having the highest value for Y-branched nanotubes (77%). Once tetracycline is added to anodized samples (NT_1s/TE and NT_2s/TE), the corrosion rate values decreased while the protective efficiency increased by 80%.

3.5.2. Impedance Diagrams

Electrochemical impedance spectroscopy (EIS) is an additional method for evaluating a material's corrosion resistance and corrosion mechanism in addition to polarization. The processes at the Ti/NT/electrolyte interface are illustrated in the EIS spectra. The Nyquist diagrams corresponding to the analyzed samples are shown in Figure 6. A smaller semicircle diameter in a Nyquist plot denotes a material with less corrosion resistance. The smallest semicircle is for unmodified Ti sample. NT_2s/TE sample showed the highest resistance to corrosion, possessing a higher semi-circle diameter compared to the remaining specimens. These observations are in accordance with Tafel polarization results.

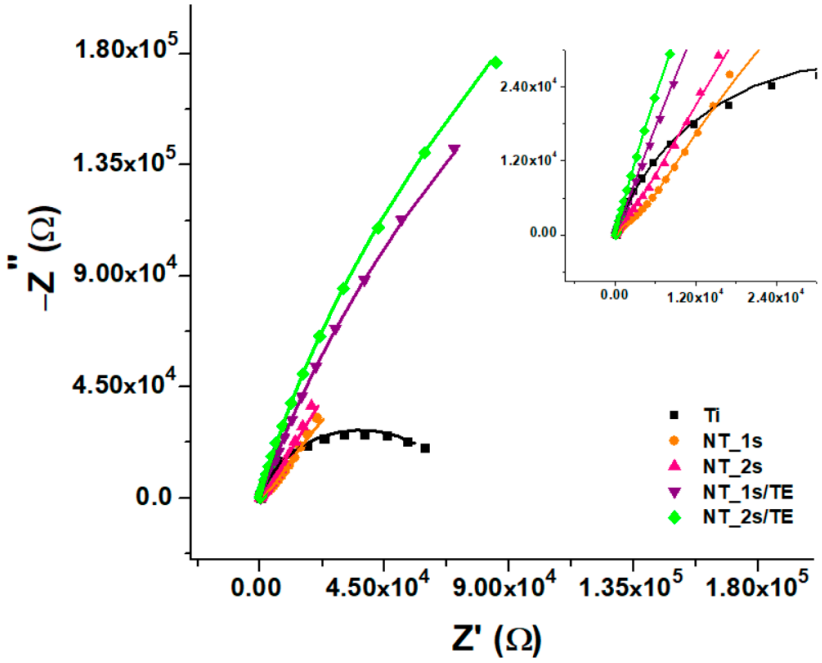

Figure 6. EIS diagrams of the analyzed samples.

The EIS diagrams were processed with the assistance of Nova 1.1 software, utilizing the equivalent circuits illustrated in Figure 7. For the substrate (titanium), a simple circuit consisting of the solution resistance (R_s) and a circuit corresponding to the barrier oxide layer were used (Figure 7a). This circuit is composed of a resistance (R_{oxide}) in parallel with a constant phase element (CPE_{oxide}) corresponding to the electrical double layer at the Ti/NaCl 0.9% interface. When immersed in solutions, an oxide layer, known as a barrier oxide, is formed on the surface of titanium. For the modified samples, the circuit from Figure 7b was used. This is made of the solution resistance ($R_{solution}$), a specific circuit for the oxide layer and a specific circuit for the coating. The produced chi-square value was within the range of 0.01–0.07 for almost all the samples, signifying that the proposed circuits are a sufficient representation of the processes by fitting the data effectively.

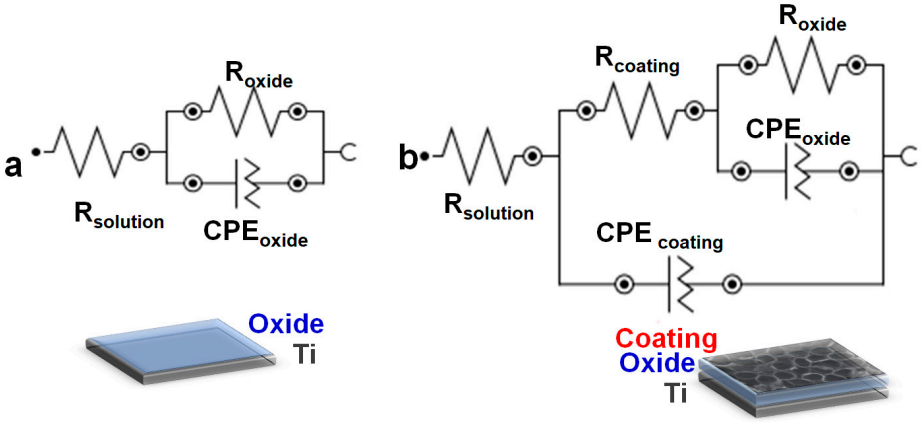

Figure 7. Equivalent circuits for EIS diagrams: (**a**) Ti substrate and (**b**) coated samples.

The equivalent circuit parameters for the analyzed samples are represented in Table 4. It is observed that for the solution (0.9% NaCl), similar resistance values were found. The modified samples exhibit a higher resistance (R_{oxide}) in the barrier oxide layer compared to that of titanium. This layer has a pseudocapacitive character because N has values lower than 1. The NT_ 2s sample has a higher resistance compared to NT_1s, due to the slightly different morphology of the nanotubes, visible in the SEM images. The nanotube layer

increases its resistance ($R_{coating}$) after immersion in tetracycline, observed for both NT_1s and NT_2s samples. The value of N indicates a pseudocapacitive behavior for this layer as well. Increasing $R_{coating}$ creates an extra diffusion barrier against corrosion and prevents the solutes ions from discharging.

Table 4. Values obtained by EIS technique.

Parameters/ Samples	R_S (Ω)	$R_{coating}$ (Ω)	$CPE_{coating}$		R_{oxide} (Ω)	CPE_{oxide}		X^2
			Y_0 ($S \times s^n$)	N		Y_0 ($S \times s^n$)	N	
Ti	120	-	-	-	72×10^3	6.2×10^{-5}	0.83	0.2
NT_1s	150	7.5×10^3	40×10^{-6}	0.75	300×10^3	7.9×10^{-5}	0.71	0.01
NT_2s	110	26.3×10^3	58×10^{-6}	0.74	990×10^3	4.0×10^{-5}	0.83	0.01
NT_1s/TE	120	29.8×10^3	32×10^{-6}	0.80	984×10^3	11×10^{-5}	0.85	0.02
NT_2s/TE	127	75.7×10^3	21×10^{-6}	0.85	890×10^3	9×10^{-5}	0.87	0.07

3.5.3. Cyclic Voltammetry

The cyclic voltammetry curves registered in 0.9% NaCl using the Autolab 302 N device are shown in Figure 8. These were recorded using the Nova 1.11 software, between 1.5 V and 1 V with a scanning rate of 100 mV/sec. These curves indicate a strong corrosion resistance for all the studied electrodes, consistent with observations from the Tafel diagrams and impedance tests. The currents are higher for untreated titanium. On the return curve (cathodic curve) the current has lower values than on the anodic curve. For samples with modified surfaces, a peak at −0.75 V can be observed. This indicates that the samples are oxidizing. In the case of one-step anodized samples, the peak is less pronounced. These peaks could also be a consequence of Tetracycline antioxidant potential, mentioned in literature [38].

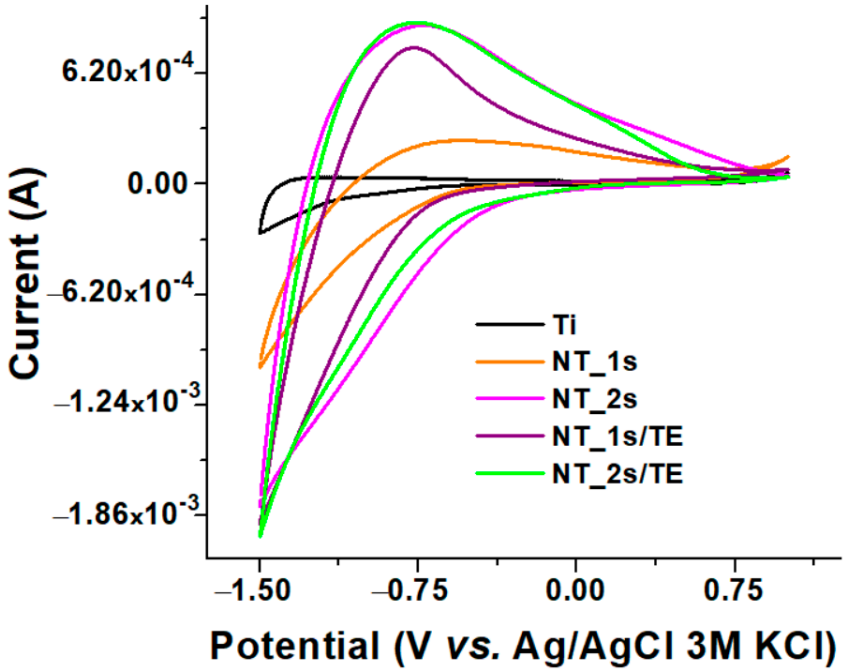

Figure 8. Cyclic voltmeters of the analyzed samples.

3.6. In Vitro Tetracycline Release

The quantity of drug absorbed in the samples was calculated as the difference between the initial amount (20 mg) and the amount of tetracycline remaining in the immersion solution. All measurements were performed in triplicate. UV–VIS analyses indicated that

the NT_1s/TE sample incorporated 1.97 ± 0.007 g/L of the initial tetracycline quantity (98.85%), while the NT_2s/TE sample incorporated 1.78 ± 0.015 g/L (98.94%).

According to the release studies, there is a rapid release in the first 1.5 days. In the case of NT_1s/TE and NT_2s/TE samples, the release of tetracycline is 23% and 20%, respectively. After 9 days, there is a slower release in the case of NT_2s / TE samples of 57% compared to NT_1s/TE samples of 88%.

The tetracycline release curves for the two samples over 9 days are seen in Figure 9. The sample NT_2s ensures a slower release over time compared to the faster NT_1s system. This behavior can be explained due to the different morphology of the TiO_2 nanotubes obtained after the anodization process. Thus, the release is similar in the first hours because the drug is released from the upper part of the nanotubes. Thereafter, the release is slower in nanotubes obtained in two steps due to the reduced diameter and branched structure.

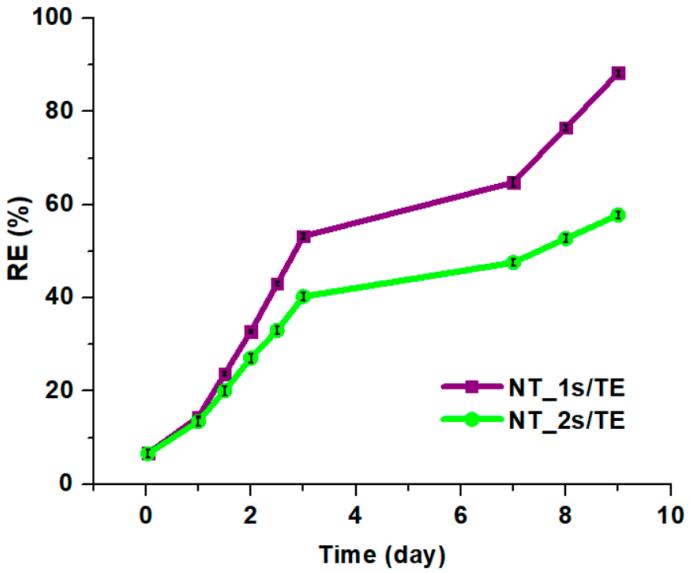

Figure 9. Drug release over time.

For fitting the tetracycline release data, three kinetic models were used: zero-order, first-order, and the Higuchi model. Table 5 presents the kinetic parameters obtained for each mathematical model: the correlation coefficient (R^2) and the rate constant (k). The mathematical model with the highest correlation coefficient (R^2) was selected as the best kinetic model for tetracycline release data.

Table 5. Kinetic parameters.

Sample	Zero Order		First Order		Higuchi	
	R^2	k_0	R^2	R^2	k_0	R^2
NT_1s/TE	0.926	8.1781	0.919	0.198	0.947	29.482
NT_2s/TE	0.893	5.098	0.997	0.088	0.953	18.773

The release of tetracycline is carried out according to the Higuchi model in both systems (according to R^2). Therefore, encapsulating tetracycline in NT_2s is favorable due to the drug's lower dose. This ensures a decrease in side effects as well as a long-lasting therapeutic effect.

3.7. Antibacterial Activity

The microorganisms used in this study were chosen due to their high pathogenicity and the fact that they are among the most common bacteria that give nosocomial infections [39,40]. Many of the infections in hospitals are those with *Staphylococcus aureus* (*S. aureus*), a bacterium that can cause severe pneumonia, conjunctivitis, otitis or simply sepsis and has become extremely resistant to antibiotics in recent years [41]. In addition to *S. aureus* infections, *Escherichia coli* (*E. coli*) is responsible for many hospital infections. Frequent respiratory tract diseases caused by *E. coli* infection are also common, pneumonia may be secondary to intubation maneuvers (incorrectly manipulated orotracheal tube) or poor oral hygiene (dental prosthesis, untreated dental infections) [42,43]. In addition to the two bacteria mentioned above, *Pseudomonas aeruginosa* is a type of bacterium that is commonly found in the environment, such as in soil and water. Usually, this bacterium does not cause infections in healthy people or cause only mild infections, but people who have a weakened immune system can develop serious infections. To overcome this kind of problem, tetracycline is a commonly used solution. In the case of an implant, the drugs should be locally delivered in a controlled manner.

For the interaction between bacteria and the new created surfaces with TiO_2 nanotubes with specific morphology that delay the release of drugs, it is necessary to consider the surface energies. This parameter can significantly influence bacterial adhesion. The interaction between bacteria and surface energy is a crucial aspect in the field of microbiology, especially concerning the adhesion of bacteria to various surfaces, which is fundamental to biofilm formation and the spread of infections [44]. Surface energy is a measure of how the surface molecules interact with the environment. High surface energy materials, like glass or certain metals, tend to be hydrophilic and can have stronger interactions with bacterial cells, which are generally hydrophilic due to their water-containing cytoplasm and hydrophilic cell wall components [45]. The initial interaction between bacteria and a surface is typically a physical process, where the bacteria are reversibly attached to the surface. Over time, this can become a stronger, irreversible attachment as the bacteria produce extracellular polymeric substances (EPS), leading to biofilm formation [46–48].

In the context of preventing bacterial growth and biofilm formation on medical devices, surfaces are often engineered to modify the surface energy or are coated with materials that modify the surface energy. Additionally, surface texture and chemistry can be manipulated to create anti-adhesive or bactericidal properties.

The coating created in this study has been characterized by a high surface energy. However, their antibacterial effect is amplified by the presence of tetracycline that is progressively released from the nanotubes. The results are presented in Figure 10.

By the titanium surface nanostructuring, an increase in the antibacterial effect of up to 15% is observed, this being also demonstrated in our previous study [4]. This can be influenced by the surface morphology and surface energy, which change when TiO_2 nanotubes are deposited on the surface.

Also, by incorporating tetracycline there is an increase in the antibacterial effect up to 55%. This could be related to the antibiotic's action. The antibacterial effect of the nanostructured surfaces is similar, which can be attributed to the same release on the first day. After 9 days, an increase in antibacterial effect for Y-branched nanotubes is expected. Thus, the morphology and chemistry of the surface, as well as the presence of the antibiotic, determine an improved antibacterial effect for implantable surfaces.

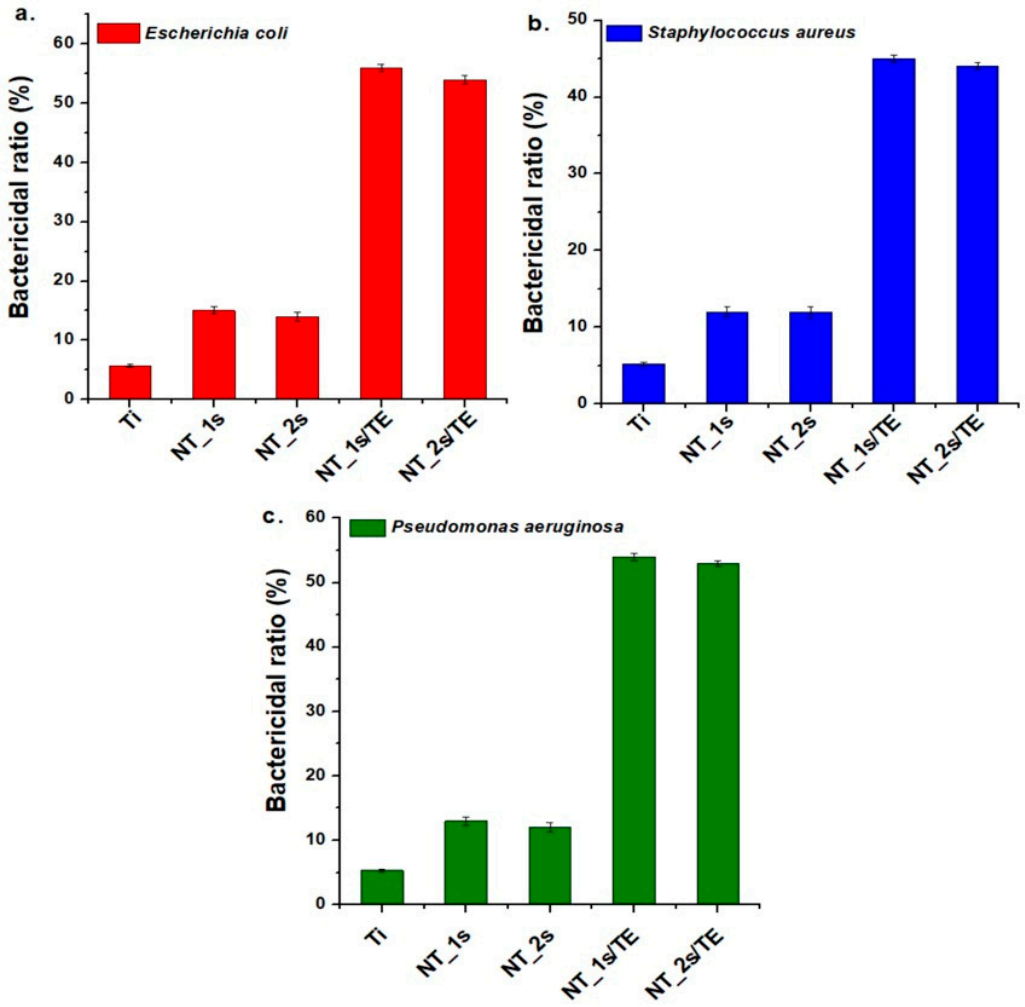

Figure 10. Bactericidal ratio after 18 h of bacteria incubation.

4. Conclusions

This study demonstrates a method for fabricating open-ended Y branched TiO_2 nanotubes by varying the anodization conditions, named NT_2s. They were created by two anodization steps. They were compared with the ones prepared in one step. The first indication of a different nanotubes was current—time curves recorded during anodizing, where the load values were higher for NT_2s. SEM images revealed that nanotubes had organized pores, like "honeycombs", were vertically aligned, and were uniformly dispersed. The NT_2s trunks are made up of big sized nanotubes with outer diameters ~ 100 nm and the inner diameter ~60 nm, while the branches are made up of small, very thin small sized nanotubes. In both cases, the length of the nanotubes is in the order of micrometers. They were loaded with Tetracycline by immersion.

According to Raman spectra, the anodized samples have both anatase and rutile peaks. For NT_1s/TE and NT_2s/TE samples, both tetracycline and TiO_2 allotropic forms were found.

All samples had hydrophilic character. After embedding the tetracycline, NT_1s/TE and NT_2s/TE had slightly lower water contact angle values and showed the highest surface energy.

According to the electrochemical test, anodized samples had less susceptibility to corrosion compared with Ti, the protection efficiency being above 60%, having the highest value for Y-branched nanotubes (77%). Once tetracycline was added to anodized samples (NT_1s/TE and NT_2s/TE), the corrosion rate values decreased while the protective efficiency increased by 80%.

The tetracycline release curves for the two samples were recorded over a period of nine days. In both systems (NT_1s/TE and NT_2s/TE), tetracycline is released in accordance with the Higuchi model. The sample NT_2s guarantees a slower release over time while the NT_1s system operates faster. Tetracycline's lower dose makes it advantageous to encapsulate it in NT_2s. This guarantees both a reduction in adverse effects and a sustained therapeutic benefit.

Tetracycline increased the antibacterial action by up to 55%. Due to the identical release on the first day, the nanostructured surfaces had comparable antibacterial effects. It is anticipated that the antibacterial activity of Y-branched nanotubes will rise after nine days, and future studies will be performed. As future perspectives, investigations will be performed to evaluate the stability and sustained drug release over an extended period, particularly under the influence of electrical stimulation. Moreover, there are plans for in vivo assessments using human cells to observe the formed interactions and gain comprehensive insights into the biocompatibility of the newly developed surfaces. Future research will also include the tetracycline release from various TiO_2 nanostructures in Fusayama simulant saliva, which has a pH of 5.5.

Author Contributions: Conceptualization, A.G.P., V.P. and C.D.; methodology, A.G.P., V.P. and C.D.; software, A.G.P. and C.D.; investigation, A.G.P., V.P., N.B., C.U., S.P. and C.D.; writing—original draft preparation, A.G.P.; writing—review and editing, A.G.P., N.B., C.U., S.P. and C.D.; visualization, A.G.P., S.P. and C.D. All authors have read and agreed to the published version of the manuscript.

Funding: This research received no external funding.

Data Availability Statement: Data available in a publicly accessible repository. The data presented in this study are openly available in [repository name e.g., FigShare] at [doi], reference number [reference number].

Conflicts of Interest: The authors declare no conflict of interest.

References

1. Bottino, M.C.; Münchow, E.A.; Albuquerque, M.T.P.; Kamocki, K.; Shahi, R.; Gregory, R.L.; Chu, T.G.; Pankajakshan, D. Tetracycline-incorporated polymer nanofibers as a potential dental implant surface modifier. *J. Biomed. Mater. Res. Part B Appl. Biomater.* **2017**, *105*, 2085–2092. [CrossRef] [PubMed]
2. Olaru, A.G.; Butculescu, V.; Dumitriu, C.; Badea, N.; Popescu, S.; Ungureanu, C.; Pirvu, C. Biopolymers as intermediate layers for amoxicillin grafting on antibacterial surface. *Surf. Interfaces* **2022**, *33*, 102224. [CrossRef]
3. Păun, A.G. TiO_2 Surfaces Modification for Amoxicillin Release Used in Dental Implantology. *UPB Sci. Bull. Ser. B* **2023**, *85*, 71–84.
4. Păun, A.G.; Popescu, S.; Ungureanu, C.; Trusca, R.; Pirvu, C. Reduced TiO_2 Nanotubes/Silk Fibroin/ZnO as a Promising Hybrid Antibacterial Coating. *ChemPlusChem* **2023**, e202300450. [CrossRef] [PubMed]
5. Wang, Q.; Huang, J.Y.; Li, H.Q.; Zhao, A.Z.; Wang, Y.; Zhang, K.Q.; Sun, H.T.; Lai, Y.K. Recent advances on smart TiO(2) nanotube platforms for sustainable drug delivery applications. *Int. J. Nanomed.* **2017**, *12*, 151–165. [CrossRef] [PubMed]
6. Bottino, M.C.; Munchow, E.A.; Maria, T.; Pankajakshan, D. Tetracycline-incorporated nanofibrous coating on titanium to prevent early implant infection and enhance cell response. In Proceedings of the 10th World Biomaterials Congress, Montreal, QC, Canada, 17–22 May 2016.
7. Tong, S.; Sun, X.; Wu, A.; Guo, S.; Zhang, H. Improved biocompatibility of TiO_2 nanotubes via co-precipitation loading with hydroxyapatite and gentamicin. *Coatings* **2021**, *11*, 1191. [CrossRef]
8. Wang, Q.; Huang, J.Y.; Li, H.Q.; Chen, Z.; Zhao, A.Z.; Wang, Y.; Zhang, K.Q.; Sun, H.T.; Al-Deyab, S.S.; Lai, Y.K. TiO(2) nanotube platforms for smart drug delivery: A review. *Int. J. Nanomed.* **2016**, *11*, 4819–4834. [CrossRef]
9. Popat, K.C.; Leoni, L.; Grimes, C.A.; Desai, T.A. Influence of engineered titania nanotubular surfaces on bone cells. *Biomaterials* **2007**, *28*, 3188–3197. [CrossRef]
10. Liu, Z.; Liu, Y.; Liu, S.; Wang, D.; Jin, J.; Sun, L.; Wang, Q.; Yi, Z. The effects of TiO_2 nanotubes on the biocompatibility of 3D printed Cu-bearing TC4 alloy. *Mater. Des.* **2021**, *207*, 109831. [CrossRef]
11. Turu, I.C.; Bayraktar, S.; Akgul, B.; Ilhan-Sungur, E.; Abamor, E.S.; Cansever, N. Formation of TiO_2 nanotubes and deposition of silver nanoparticle and reduced graphene oxide: Antibacterial and biocompatibility behavior. *Surf. Coat. Technol.* **2023**, *470*, 129866. [CrossRef]
12. Xuan, B.; Li, L.; Zhang, H.; Liu, Z.; Luo, R.; Yang, W.; Wang, W. Antibacterial and anti-inflammatory effects of PGLa-loaded TiO_2 nanotube arrays. *Front. Chem.* **2023**, *11*, 1210425. [CrossRef] [PubMed]
13. Chen, B.; Lu, K. Hierarchically Branched Titania Nanotubes with Tailored Diameters and Branch Numbers. *Langmuir* **2012**, *28*, 2937–2943. [CrossRef] [PubMed]

14. Anitha, V.C.; Banerjee, A.N.; Joo, S.W.; Min, B.K. Barrier-oxide layer engineering of TiO_2 nanotube arrays to get single- and multi-stage Y-branched nanotubes: Effect of voltage ramping and electrolyte conductivity. *Mater. Sci. Eng. B* **2015**, *195*, 1–11. [CrossRef]
15. Sun, L.; Xu, J.; Sun, Z.; Zheng, F.; Liu, C.; Wang, C.; Hu, X.; Xia, L.; Liu, Z.; Xia, R. Decreased Porphyromonas gingivalis adhesion and improved biocompatibility on tetracycline-loaded TiO_2 nanotubes: An in vitro study. *Int. J. Nanomed.* **2018**, *13*, 6769–6777. [CrossRef]
16. Plodinec, M.; Grčić, I.; Willinger, M.G.; Hammud, A.; Huang, X.; Panžić, I.; Gajović, A. Black TiO_2 nanotube arrays decorated with Ag nanoparticles for enhanced visible-light photocatalytic oxidation of salicylic acid. *J. Alloys Compd.* **2019**, *776*, 883–896. [CrossRef]
17. Draghi, L.; Preda, V.; Moscatelli, M.; Santin, M.; Chiesa, R. Gentamicin-Loaded TiO_2 Nanotubes as Improved Antimicrobial Surfaces for Orthopedic Implants. *Front. Mater.* **2020**, *7*, 233. [CrossRef]
18. Păun, A.G.; Dumitriu, C.; Ungureanu, C.; Popescu, S. Silk Fibroin/ZnO Coated TiO_2 Nanotubes for Improved Antimicrobial Effect of Ti Dental Implants. *Materials* **2023**, *16*, 5855. [CrossRef]
19. Shahi, R.G.; Albuquerque, M.T.P.; Münchow, E.A.; Blanchard, S.B.; Gregory, R.L.; Bottino, M.C. Novel bioactive tetracycline-containing electrospun polymer fibers as a potential antibacterial dental implant coating. *Odontology* **2017**, *105*, 354–363. [CrossRef]
20. Park, J.B. Treatment of peri-implantitis with deproteinised bovine bone and tetracycline: A case report. *Gerodontology* **2012**, *29*, 145–149. [CrossRef]
21. Im, S.Y.; Kim, K.M.; Kwon, J.S. Antibacterial and Osteogenic Activity of Titania Nanotubes Modified with Electrospray-Deposited Tetracycline Nanoparticles. *Nanomaterials* **2020**, *10*, 1093. [CrossRef]
22. Wychowański, P.; Starzyńska, A.; Adamska, P.; Słupecka-Ziemilska, M.; Sobocki, B.K.; Chmielewska, A.; Wysocki, B.; Alterio, D.; Marvaso, G.; Jereczek-Fossa, B.A.; et al. Methods of Topical Administration of Drugs and Biological Active Substances for Dental Implants—A Narrative Review. *Antibiotics* **2021**, *10*, 919. [CrossRef] [PubMed]
23. Irodia, R. Enhanced photocatalytic degradation of tetracycline by TiO_2 nanotubes coated with TiO_2 nanofibers. *UPB Sci. Bull. Ser. B Chem. Mater. Sci.* **2023**, *85*, 63–76.
24. Dumitriu, C.; Pirvu, C. Electrochemical studies on TiO_2 nanotubes modified Ti electrodes. *Univ. Politeh. Buchar. Sci. Bull. Ser. B-Chem. Mater. Sci.* **2012**, *74*, 93–106.
25. Hata, T.; Kitazaki, Y.; Saito, T. Estimation of the Surface Energy of Polymer Solids. *J. Adhes.* **1987**, *21*, 177–194. [CrossRef]
26. Ansari, M.; Khan, H.; Khan, A. Evaluation of antibacterial activity of silver nanoparticles against MSSA and MSRA on isolates from skin infections. *Biol. Med.* **2011**, *3*, 141–146.
27. Jaiswal, S.; Duffy, B.; Jaiswal, A.K.; Stobie, N.; McHale, P. Enhancement of the antibacterial properties of silver nanoparticles using beta-cyclodextrin as a capping agent. *Int. J. Antimicrob. Ag.* **2010**, *36*, 280–283. [CrossRef] [PubMed]
28. Ionita, D.; Grecu, M.; Ungureanu, C.; Demetrescu, I. Modifying the TiAlZr biomaterial surface with coating, for a better anticorrosive and antibacterial performance. *Appl. Surf. Sci.* **2011**, *257*, 9164–9168. [CrossRef]
29. Macák, J.M.; Tsuchiya, H.; Schmuki, P. High-aspect-ratio TiO_2 nanotubes by anodization of titanium. *Angew. Chem. Int. Ed.* **2005**, *44*, 2100–2102. [CrossRef]
30. Li, Y.; Yang, Y.; Li, R.; Tang, X.; Guo, D.; Qing, Y.; Qin, Y. Enhanced antibacterial properties of orthopedic implants by titanium nanotube surface modification: A review of current techniques. *Int. J. Nanomed.* **2019**, *14*, 7217–7236. [CrossRef]
31. Zakir, O.; Idouhli, R.; Elyaagoubi, M.; Khadiri, M.; Aityoub, A.; Koumya, Y.; Rafqah, S.; Abouelfida, A.; Outzourhit, A. Fabrication of TiO_2 Nanotube by Electrochemical Anodization: Toward Photocatalytic Application. *J. Nanomater.* **2020**, *2020*, 4745726. [CrossRef]
32. Wan, J.; Yan, X.; Ding, J.; Wang, M.; Hu, K. Self-organized highly ordered TiO_2 nanotubes in organic aqueous system. *Mater. Charact.* **2009**, *60*, 1534–1540. [CrossRef]
33. Hardcastle, F. Raman spectroscopy of titania (TiO_2) nanotubular water-splitting catalysts. *J. Ark. Acad. Sci.* **2011**, *65*, 43–48.
34. Challagulla, S.; Tarafder, K.; Ganesan, R.; Roy, S. Structure sensitive photocatalytic reduction of nitroarenes over TiO 2. *Sci. Rep.* **2017**, *7*, 8783. [CrossRef] [PubMed]
35. Dhakal, S.; Chao, K.; Huang, Q.; Kim, M.; Schmidt, W.; Qin, J.; Broadhurst, C.L. A Simple Surface-Enhanced Raman Spectroscopic Method for on-Site Screening of Tetracycline Residue in Whole Milk. *Sensors* **2018**, *18*, 424. [CrossRef] [PubMed]
36. Muhammad, M.; Yan, B.; Yao, G.; Chao, K.; Zhu, C.; Huang, Q. Surface-enhanced Raman spectroscopy for trace detection of tetracycline and dicyandiamide in milk using transparent substrate of ag nanoparticle arrays. *ACS Appl. Nano Mater.* **2020**, *3*, 7066–7075. [CrossRef]
37. Pawłowski, Ł.; Wawrzyniak, J.; Banach-Kopeć, A.; Cieślik, B.M.; Jurak, K.; Karczewski, J.; Tylingo, R.; Siuzdak, K.; Zieliński, A. Antibacterial properties of laser-encapsulated titanium oxide nanotubes decorated with nanosilver and covered with chitosan/Eudragit polymers. *Biomater. Adv.* **2022**, *138*, 212950. [CrossRef] [PubMed]
38. Kładna, A.; Michalska, T.; Berczyński, P.; Kruk, I.; Aboul-Enein, H.Y. Evaluation of the antioxidant activity of tetracycline antibiotics in vitro. *Lumin. J. Biol. Chem. Lumin.* **2012**, *27*, 249–255. [CrossRef] [PubMed]
39. Tolera, M.; Abate, D.; Dheresa, M.; Marami, D. Bacterial Nosocomial Infections and Antimicrobial Susceptibility Pattern among Patients Admitted at Hiwot Fana Specialized University Hospital, Eastern Ethiopia. *Adv. Med.* **2018**, *2018*, 2127814. [CrossRef]
40. Khan, H.A.; Ahmad, A.; Mehboob, R. Nosocomial infections and their control strategies. *Asian Pac. J. Trop. Biomed.* **2015**, *5*, 509–514. [CrossRef]

41. Mason, R.J.; Broaddus, V.C.; Martin, T.R.; King, T.E.; Schraufnagel, D.; Murray, J.F.; Nadel, J.A. *Murray and Nadel's Textbook of Respiratory Medicine E-Book: 2-Volume Set*; Elsevier Health Sciences: Amsterdam, The Netherlands, 2010.
42. Harrington, S.M.; Dudley, E.G.; Nataro, J.P. Pathogenesis of enteroaggregative Escherichia coli infection. *FEMS Microbiol. Lett.* **2006**, *254*, 12–18. [CrossRef]
43. Fleckenstein, J.M.; Hardwidge, P.R.; Munson, G.P.; Rasko, D.A.; Sommerfelt, H.; Steinsland, H. Molecular mechanisms of enterotoxigenic Escherichia coli infection. *Microbes Infect.* **2010**, *12*, 89–98. [CrossRef] [PubMed]
44. Tuson, H.H.; Weibel, D.B. Bacteria-surface interactions. *Soft Matter* **2013**, *9*, 4368–4380. [CrossRef] [PubMed]
45. Packham, D.E. Surface energy, surface topography and adhesion. *Int. J. Adhes. Adhes.* **2003**, *23*, 437–448. [CrossRef]
46. Renner, L.D.; Weibel, D.B. Physicochemical regulation of biofilm formation. *MRS Bull.* **2011**, *36*, 347–355. [CrossRef] [PubMed]
47. Notley, S.M.; Crawford, R.J.; Ivanova, E.P. Bacterial interaction with graphene particles and surfaces. In *Advances in Graphene Science*; IntechOpen: Rijeka, Croatia, 2013; pp. 99–118.
48. Berne, C.; Ducret, A.; Hardy, G.G.; Brun, Y.V. Adhesins Involved in Attachment to Abiotic Surfaces by Gram-Negative Bacteria. *Microbiol. Spectr.* **2015**, *3*, 163–199. [CrossRef]